

Hysteresis Models of Dynamic Mode Atomic Force Microscopes: Analysis and Identification

Michele Basso, Donatello Materassi

Dipartimento di Sistemi e Informatica, Università di Firenze

via S. Marta, 3, I-50139 Firenze (Italy)

fax: +39-0554796363 tel: +39-0554796524

(basso@dsi.unifi.it / materassi@dsi.unifi.it)

Murti Salapaka

Electrical Engineering Department, Iowa State University

3128, Coover Hall, Ames, Iowa - 50011

(murti@iastate.edu)

Keywords: Atomic force microscopy; hysteresis; harmonic balance; identification; nanotechnology; Lur'e system

Abstract

A new class of models based on hysteresis functions is developed to describe atomic force microscopes operating in dynamic mode. Such models

are able to account for dissipative phenomena in the tip-sample interaction which are peculiar of this operation mode. The model analysis, which can be pursued using frequency domain techniques, provides a clear insight of specific nonlinear behaviours. Experiments show good agreement with the identified models.

1 Introduction

Physical systems showing impact phenomena are frequent in many fields [1]. Main applications occur in mechanics where macroscopic objects are considered. In this case, an impulsive approximation for interaction forces with a pure repulsive nature can often be correctly assumed. Moreover, energy losses are traditionally considered by introducing the concept of coefficient of restitution [2] [3]. However, there are many situations when this kind of approximation can not be considered satisfactory, for example when the interaction involves both attractive and repulsive forces or when the interaction can not be assumed instantaneous. The aim of this work is to exploit a hysteresis function to model the related interaction forces. This new model can be viewed as a generalization of the impulsive case and allows for the use of potential functions even if the system is dissipative. It also presents advantages when the interaction forces involve both repulsive and attractive parts or when the duration of the impact is not negligible. In addition the hysteresis model allows for the use of powerful analysis techniques, such as harmonic balance [4], which could not be used for impulsive forces. To show how the above impact model can be successfully em-

ployed, its application to an Atomic Force Microscope (AFM) is demonstrated. Specifically, we limit ourselves to the study of an AFM operating in dynamic mode, whose schematic is depicted in Figure 1: the cantilever is periodically forced by a piezo placed under its support inducing a periodic oscillation that is influenced by the interaction forces between the cantilever tip and the sample. The topography can be inferred by slowly moving the cantilever along the sample surface by means of a piezoactuator and by measuring the amplitude of the cantilever deflection through an optical lever method. A feedback controller

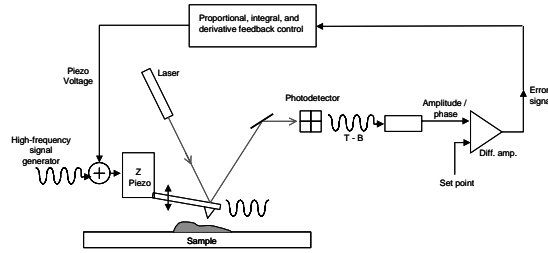


Figure 1: Schematic of a tapping-mode AFM.

driving the piezo input voltage is employed to reject variations of the separation between the sample and the tip center of oscillation due to the sample topography. In AFM, the amplitude-distance curve is not used to obtain the sample topography. It is the control-signal that is used to get the image. Therefore, the amplitude-distance curve for topography is not crucial. However, topography is not the only information one might be interested in. One of the primary uses of AFM is the study of force interactions [5]. Two methods are prevalent. The cantilever-sample offset (also termed as separation), which is a measure of the

distance of the cantilever holder and the piezo-positioner, is first reduced by the piezo positioner, where the sample surfaces approaches the cantilever-tip. In the retract phase the cantilever-sample offset is increased by using the piezo positioner. During the approach and the retract phases the cantilever deflection signal is recorded. The force felt by the cantilever, can be obtained by multiplying the deflection by its spring-constant. By plotting the force felt by the cantilever against the cantilever-sample offset the force curves are obtained. These curves are called static force curves. In dynamic force curves the cantilever is oscillated using the dither piezo. The amplitude of the first harmonic is plotted against the cantilever-sample offset during the approach and retract phases. The dynamic force curves are gentler on the sample and therefore are the preferred means of investigating samples that are soft (e. g. biological samples). One of the difficulties of using the dynamic force curve mode when compared to static force curve mode in obtaining force curves is that determining force-separation curves from the measured amplitude-separation curves is not as straightforward. In most cases, dynamic force curves are obtained by intensive numerical simulation. For example, in [6] and [7] models that accurately describe the device behaviour are proposed. In another approach, parametrized models of the tip sample interaction are assumed, the parameters identified using the amplitude-separation data, and subsequently, the force-curve data is generated using the identified model. In [8] an identification algorithm of the force-curve is obtained by the numerical computation of an explicit integral equation. There are only few attempts in the literature on analytical results.

Analytical results can be found in [9], where a simple impulsive impact model is developed. However, since the employed model neglects attractive forces, it does not seem able to explain some important characteristics of the tip-sample interaction observed in experiments.

In this work, we develop a complete frequency analysis of a dynamic-mode AFM exploiting the proposed hysteresis description and taking into account attractive forces in the sample-cantilever interaction. The main feature of the proposed model is to provide results without the means of numerical simulations, for example evaluating the separation-amplitude curve for a large class of interaction forces comprising some of the common potential functions studied in the literature, such as the classical Lennard-Jones potential [10]. Other peculiar attractive features of the proposed class of models are: *i*) it can easily account for energy losses; *ii*) it is suited for nonlinear frequency-domain identification techniques such as those proposed in [7] and [11]; *iii*) it facilitates to study some structural properties of the system such as bifurcation phenomena experimentally observed exploiting frequency domain techniques as in [12]. Identification results based on experimental data are provided where the hysteresis model gives a good qualitative and quantitative characterization of the tip-sample behaviour.

The paper is organized as follows. In Section 2 we briefly describe the general problem of modelling an impact reminding many consolidate notions for the sake of clarity. In Section 3 we exploit such a model to describe the AFM tapping-mode dynamics and in Section 4 a frequency analysis is provided us-

ing harmonic balance techniques. In Section 5 the identification procedure is described and finally in Section 6 experimental results are discussed.

2 Hysteresis functions to model a collision

Let P_1 and P_2 be two material objects with masses m_1 and m_2 , respectively, moving along the x axis, with position x_1 and x_2 ($x_1 < x_2$). We consider P_1 and P_2 subject to external forces $f_1(t)$ and $f_2(t)$ respectively, and to a mutual internal force. P_1 exerts a force on P_2 given by h_2 and P_2 exerts an equal and opposite force h_1 on P_1 . The interaction force h_i are dependent on time t , relative separation $x_1 - x_2$ and relative velocities $\dot{x}_1 - \dot{x}_2$. The following dynamical relations describe the system

$$\begin{cases} m_1 \ddot{x}_1 = f_1(t) + h_1(t, x_2 - x_1, \dot{x}_2 - \dot{x}_1) \\ m_2 \ddot{x}_2 = f_2(t) + h_2(t, x_2 - x_1, \dot{x}_2 - \dot{x}_1). \end{cases} \quad (1)$$

Earlier interaction models usually neglected dissipation losses or used a constant coefficient of restitution to account for such losses. Defining $\delta := x_2 - x_1$, we suppose the interaction between the two masses is negligible outside a time interval $[t_s, t_f]$ where $\delta(t_s) = \delta(t_f)$. We intend to limit our study to the case where P_1 and P_2 get closer at the beginning, and then further. We assume that the system dynamics can be split in two different phases: an “approach phase” in the time interval $[t_s, \bar{t}]$ where $\dot{\delta} \leq 0$ and a “retract phase” in the time interval $[\bar{t}, t_f]$ where $\dot{\delta} \geq 0$. We also consider that $\delta(t)$ is a continuous function and that the set of points where $\dot{\delta} = 0$ has zero measure. The model we intend to employ in this work defines a particular form for the interaction forces and, at the same

time, allows one to generalize the case of constant coefficient of restitution, not only for an instantaneous impact time. In addition, it presents advantages in the study of impacting systems with periodic behaviours. The interaction force assumes two different forms during the approach and the retract phases

$$h(\delta, \dot{\delta}) := \begin{cases} h^+(\delta) & \text{if } \dot{\delta} > 0 \\ h^-(\delta) & \text{if } \dot{\delta} < 0. \end{cases} \quad (2)$$

The simplicity of the dependence of h on the sign of $\dot{\delta}$ leads to a tractable analysis while capturing the prominent features of finite time that can have both attractive as well as repulsive forces.

If h^+ and h^- are integrable, then the potential functions U^+ and U^- can be introduced with

$$\begin{aligned} U^+(\delta) &= - \int_{\delta(t_s)}^{\delta} h^+(x) dx \\ U^-(\delta) &= - \int_{\delta(t_s)}^{\delta} h^-(x) dx. \end{aligned} \quad (3)$$

As $h^-(\delta) > h^+(\delta) \quad \forall \delta < \delta(t_s)$, we have also that $U^-(\delta) > U^+(\delta) \quad \forall \delta < \delta(t_s)$.

Considering the instant \bar{t} when the relative distance $\delta(t)$ is the smallest, we can state that the potential interaction energy is $U^-(t)$ if $t < \bar{t}$, while it is $U^+(t)$ if $t > \bar{t}$. At any instant the interaction force is conservative except at $t = \bar{t}$ when the relative velocity is zero and we have an “instantaneous” energy variation ΔE equal to

$$\Delta E = U^-(\delta(\bar{t})) - U^+(\delta(\bar{t})). \quad (4)$$

The energy lost in the impact can be interpreted as the area between the curves $h^-(\delta)$ and $h^+(\delta)$ in the interval $[\delta(\bar{t}), \delta(t_s)]$. In the next section we will show how this class of hysteresis functions can be exploited to analyze and identify

tip-sample interactions in AFMs.

3 AFM model

AFM cantilevers can be modeled as a feedback interconnection of a linear system \mathcal{L} and a nonlinear static function h as depicted in Figure 2. Models with this

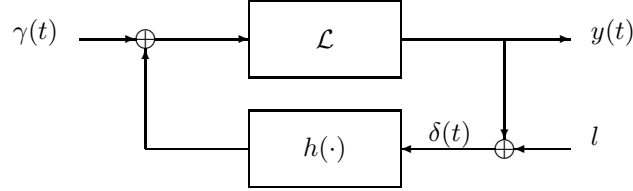


Figure 2: A feedback interconnection of a linear system and a nonlinear static function.

peculiar structure are well-known as Lur'e models [4]. The system equation can be conveniently written using the symbolic form

$$y(t) = L \left(\frac{d}{dt} \right) [h(\delta(t), \dot{\delta}(t)) + \gamma(t)] \quad (5)$$

where $y(t)$ is the measured output (that is the cantilever tip deflection), l , apart an additive constant, is the separation, $\delta(t) = y(t) + l$ represents the tip-sample distance, and $\gamma(t)$ is the external periodic forcing

$$\gamma(t) = \Gamma \cos(\omega t + \phi) \quad .$$

The subsystem \mathcal{L} describes the free cantilever dynamics, whose frequency response $L(i\omega)$ can be precisely identified using thermal noise or a simple frequency sweep excitation when the sample is absent [13].

The feedback subsystem h accounts for the sample interaction force, which is a highly nonlinear function of the tip-sample distance δ . Modeling h is still a challenging task. The main difficulty lies in the choice of a suitable class of functions to describe the force potential. It is a common choice to consider h as the sum of a conservative force h_{con} and a dissipative one h_{dis}

$$h(\delta, \dot{\delta}) = h_{con}(\delta) + h_{dis}(\delta, \dot{\delta}) \quad (6)$$

giving to h_{dis} a simple form to allow easy computation [14]. Also in [14] it is proposed

$$h_{dis}(\delta, \dot{\delta}) = \Gamma(\delta)\dot{\delta} \quad (7)$$

where Γ represents a sort of damping coefficient.

In this paper we consider the following class of hysteresis functions which generalizes the one presented in [15]

$$h(\delta, \dot{\delta}) = \begin{cases} \sum_{n=1}^N K_n^- h_n(\delta) & \text{if } \dot{\delta} < 0 \\ \sum_{n=1}^N K_n^+ h_n(\delta) & \text{if } \dot{\delta} \geq 0 \end{cases} \quad (8)$$

where $h_n(\delta)$ are a class of suitable non-negative functions where the dependence on $\dot{\delta}$ occurs in h considering only its sign as described in the previous section. Relation (8) represents a vector space of hysteresis functions made of two different positional forces: the first one acts when the tip and the sample are approaching and the second one when they are getting further. In order to

make the interaction described by $h(\delta, \dot{\delta})$ dissipative, some constraints on the parameters K_n^+ and K_n^- can be imposed. For example, the condition

$$K_n^- \geq K_n^+ \quad (9)$$

makes every base element h_n dissipative.

In our analysis, we will consider two special cases of this hysteretic interaction. This way of modeling dissipations has already been proposed in [16] and has been successfully exploited by [15] in an identification procedure.

3.1 Piecewise interaction force

The first class of potential functions we treat contains the functions $h(\cdot)$ in the form (8) where $N = 2$ and

$$h_n(\delta) = \begin{cases} 0 & \text{if } \delta \geq 0 \\ |\delta|^{n-1} & \text{if } \delta < 0. \end{cases} \quad (10)$$

In Figure 3 the shape of such a kind of functions is depicted. Since $\delta = y + l$, here the parameter l models the cantilever deflection at which the tip-sample interaction forces become effective.

3.2 Lennard-Jones-like interaction force

The Lennard-Jones potential

$$h(\delta) = \frac{K_{n_a}}{\delta^{n_a}} + \frac{K_{n_r}}{\delta^{n_r}} \quad n_a < n_r \in \mathcal{N}; \quad K_{n_a}, K_{n_r} \in \mathcal{R} \quad (11)$$

is a common choice when fitting statically measured curves often used as a model of interaction potential between atoms (see [5]) We consider a generalization of

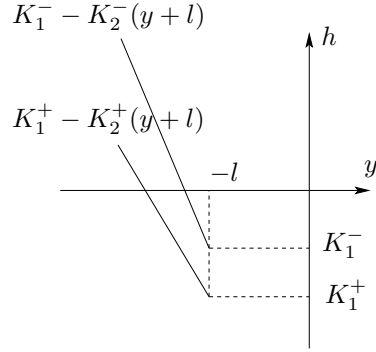


Figure 3: Interaction force modeled by a piecewise linear function.

the Lennard-Jones Potential in the form (8) where

$$h_n(y) = \frac{1}{\delta^n}. \quad (12)$$

The parameter l represents the cantilever deflection where the interaction force

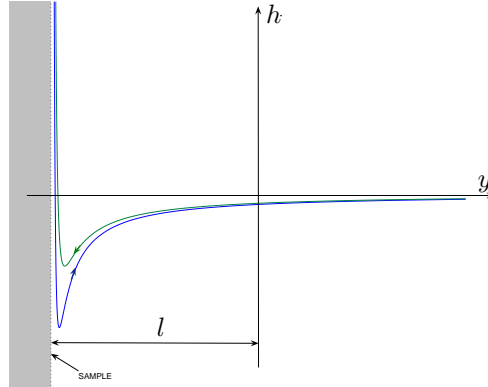


Figure 4: Sketch of a Lennard-Jones-like interaction with hysteresis.

becomes infinitely large (Figure 4). The choice of this class of functions is

motivated by its simplicity and also by the fact that long-range dissipative interfacial forces has already been successfully modelled using a time-dependent power law where the strength of the force depends only on whether the probe approaches or retracts away from the sample. [15]

4 Frequency Analysis via Harmonic Balance

The linear part of the Lur'e system given by \mathcal{L} in (5) typically shows a sharp filtering effect beyond the first resonance peak because of a very high quality factor of the cantilever. Indeed, it is experimentally observed that the cantilever trajectory has a quasi-sinusoidal behaviour. The cantilever-tip motion can be approximated by

$$y(t) \simeq y_1(t) := \text{Re}[A + Be^{i\omega t}] = A + B \cos(\omega t) \quad (13)$$

The corresponding output of the nonlinear hysteresis block can be approximated as

$$h(y + l, \dot{y}) \simeq h(y_1 + l, \dot{y}_1) \simeq \text{Re} [N_0 A + N_1 B e^{i\omega t}] \quad (14)$$

where

$$\begin{cases} N_0 = N_0(A, B, \omega) := \frac{1}{A} \frac{1}{T} \int_0^T h(y_1(t) + l, \dot{y}_1(t)) dt \\ N_1 = N_1(A, B, \omega) := \frac{1}{B} \frac{2}{T} \int_0^T h(y_1(t), \dot{y}_1(t)) e^{-i\omega t} dt \end{cases} \quad (15)$$

are the constant and harmonic gains of the nonlinear block also known as the describing functions of the nonlinearity [4]. We remark that $N_0 A$ and $N_1 B$ are the first two Fourier coefficients of $h(y_1(t) + l, \dot{y}_1(t))$, thus expression (15) represents a first order harmonic truncation. For the general class of hysteretic

force models introduced, we obtain

$$\begin{aligned} N_0 &= \frac{1}{2\pi A} \sum_{n=1}^N \left(\int_{-\pi}^0 K_n^+ h_n(l + A + B \cos \tau) d\tau + \int_0^{+\pi} K_n^- h_n(l + A + B \cos \tau) d\tau \right) = \\ &= \frac{1}{2\pi A} \sum_{n=1}^N \Sigma_n \int_0^{+\pi} h_n[B(q + \cos \tau)] d\tau \end{aligned}$$

where

$$\Sigma_n := K_n^- + K_n^+ \quad (16)$$

and

$$q := \frac{l + A}{B} . \quad (17)$$

Similarly, we find for N_1

$$\begin{aligned} N_1 &= \frac{1}{\pi B} \sum_{n=1}^N \left(\int_{-\pi}^0 K_n^+ h_n[B(q + \cos \tau)] e^{-i\tau} d\tau + \int_0^{+\pi} K_n^- h_n[B(q + \cos \tau)] e^{-i\tau} d\tau \right) = \\ &= \frac{1}{\pi B} \sum_{n=1}^N \left(\Sigma_n \int_0^{+\pi} h_n[B(q + \cos \tau)] \cos \tau d\tau - i \Delta_n \int_0^{+\pi} h_n[B(q + \cos \tau)] \sin \tau d\tau \right) \end{aligned} \quad (18)$$

where

$$\Delta_n := K_n^+ - K_n^- . \quad (19)$$

Substituting in (5), assuming a sinusoidal forcing $\gamma(t) = \text{Re}[\Gamma e^{i(\omega t + \phi)}]$, yields

$$A + B e^{i\omega t} = -L(0)N_0 A + L(i\omega)[-N_1 B + \Gamma e^{i\phi}] e^{i\omega t} \quad \forall t \quad (20)$$

or, equivalently,

$$\begin{cases} [1 + L(0)N_0(A, B)] A = 0 \\ [1 + L(i\omega)N_1(A, B)] B = L(i\omega)\Gamma e^{i\phi}. \end{cases} \quad (21)$$

Finally, we can easily decouple the variable ϕ from (21) as follows

$$\begin{cases} [1 + L(0)N_0(A, B)]A = 0 \\ |1 + L(i\omega t)N_1(A, B)|B = |L(i\omega t)|\Gamma. \\ \phi = \arg [L(i\omega)^{-1} + N_1(A, B)] . \end{cases} \quad (22)$$

The equations (22) represent a system of three nonlinear equations in the three unknown A, B, ϕ . By solving it, we can find the sinusoidal approximation of $y(t)$ given by (13).

4.1 Piecewise interaction model analysis

For the piecewise-linear potential described in Section 3.1 we obtain

$$\begin{cases} N_0 = \frac{1}{A} [\Sigma_1 R_1(q) + \Sigma_2 R_2(q)B] \\ N_1 = \frac{1}{B} [\Sigma_1 S_1(q) + i\Delta_1 T_1(q)] + [\Sigma_2 S_2(q) + i\Delta_2 T_2(q)] \end{cases} \quad (23)$$

where

$$\begin{aligned} R_1(q) &:= \frac{\arccos(q)}{2\pi} & R_2(q) &:= \frac{q\arccos(q) - \sqrt{1-q^2}}{2\pi} \\ S_1(q) &:= -\frac{\sqrt{1-q^2}}{\pi} & S_2(q) &:= \frac{\arccos(q) - q\sqrt{1-q^2}}{2\pi} \\ T_1(q) &:= \frac{1-q}{\pi} & T_2(q) &:= -\frac{(1-q)^2}{2\pi} \end{aligned}$$

Finally, by the substitutions

$$\chi(q) := \Sigma_1 R_1(q) \quad \Omega(q) := \Sigma_2 R_2(q)$$

$$\Phi(q) := \Sigma_1 S_1(q) + i\Delta_1 T_1(q) \quad \Psi(q) := \Sigma_2 S_2(q) + i\Delta_2 T_2(q)$$

we can obtain for the describing functions

$$\begin{aligned} N_0 &= \frac{1}{A} [\chi(q) + \Omega(q)B] \\ N_1 &= \frac{\Phi(q)}{B} + \Psi(q). \end{aligned}$$

In this model, the variable q represents the “penetration” of the tip into the sample. In fact, assuming as exact the first harmonic approximation, we have that for $q > 1$ the tip does not get in contact with the sample; for $q = 1$ the tip grazes the sample and for $q < 1$ the tip enters the sample. The case $q < -1$ does not have a physical meaning in this model. From (21), it is also possible to write B as a function of q . In fact

$$B = \frac{\Gamma}{|L(i\omega)^{-1} + N_1|} \quad (24)$$

implies

$$|L(i\omega)^{-1}B + BN_1|^2 = |L(i\omega)^{-1}B + \Phi + \Psi B|^2 = \Gamma^2. \quad (25)$$

The substitutions $\hat{\Phi} := \Phi$ and $\hat{\Psi} := \Psi + L(i\omega)^{-1}$ yield

$$\begin{aligned} (\hat{\Phi} + \hat{\Psi}B)(\hat{\Phi}^* + \hat{\Psi}^*B) &= \Gamma^2 \Rightarrow \\ |\hat{\Psi}|^2 B^2 + 2\text{Re}[\hat{\Phi}\hat{\Psi}^*]B + |\hat{\Phi}|^2 - \Gamma^2 &= 0. \end{aligned} \quad (26)$$

which is a simple second order algebraic equation whose roots are

$$B(q) = \frac{-\text{Re}[\hat{\Phi}\hat{\Psi}^*] \pm \sqrt{\text{Re}[\hat{\Phi}\hat{\Psi}^*]^2 - |\hat{\Psi}|^2(|\hat{\Phi}|^2 - \Gamma^2)}}{|\hat{\Psi}|^2}. \quad (27)$$

Substituting in (22) and reminding that $l = qB - A$, we can finally write

$$\begin{cases} A(q) = -L(0) [\chi(q) + \Psi(q)B(q)] \\ \phi(q) = \arg [L(i\omega)^{-1} + N_1(A, B(q))] \\ l(q) = qB(q) + L(0) [\chi(q) + \Psi(q)B(q)]. \end{cases} \quad (28)$$

The variable q (17), depends on A , B and l (see (17)), therefore equations (28) are implicit relations. System (28) can not be solved in closed form since it involves transcendental equations. However, it is possible to obtain its solution

through a conceptually easy method. Assuming that l is a known parameter of the model, it is possible by the last of (28), to determine the corresponding values of q and then A , B and ϕ by exploiting the remaining equations. In other words, we have transformed the problem of solving the whole system (21) into the easier problem of solving a single real equation in the unknown q .

Experimentally, the separation-amplitude curve is obtained by slowly moving the sample towards the cantilever and measuring both the amplitude of the first harmonic and the separation. Although it is not possible to derive an explicit analytical form for $B = B(l)$, we can give a parametric form for it. By using the “ q -explicit” equations in (28) we can consider the parametric curve

$$\begin{cases} l = l(q) \\ B = B(q) \end{cases} \quad \forall q \in \mathbf{R}. \quad (29)$$

4.2 Lennard Jones-like hysteretic model analysis

For the generic hysteretic interaction force of the class (12), we can evaluate the describing functions N_0 and N_1 of the nonlinearity h :

$$\begin{cases} N_0 &= \sum_{n=1}^N \frac{\Sigma_n}{AB^n} R_n(q) \\ N_1 &= \sum_{n=1}^N \frac{1}{B^{n+1}} [\Sigma_n S_n(q) + i \Delta_n T_n(q)] \end{cases}$$

where the functions

$$\begin{aligned} R_n(q) &:= \frac{1}{2\pi} \int_0^\pi \frac{1}{(q + \cos \tau)^n} d\tau \\ S_n(q) &:= \frac{1}{\pi} \int_0^\pi \frac{\cos \tau}{(q + \cos \tau)^n} d\tau \\ T_n(q) &:= \frac{1}{\pi} \int_0^\pi \frac{-\sin \tau}{(q + \cos \tau)^n} d\tau. \end{aligned}$$

can be analytically evaluated for any given n and $q > 1$.

Imposing harmonic balance, we get

$$\begin{cases} A = -L(0) \sum_{n=1}^N \Sigma_n \frac{R_n(q)}{B^n} \\ \left[\Gamma e^{i\phi} - \sum_{n=1}^N \frac{\Sigma_n S_n(q) + i\Delta_n T_n(q)}{B^n} \right] L(i\omega) = B. \end{cases} \quad (30)$$

The second equation of (30) can be expressed in the form

$$L(i\omega) \Gamma e^{i\phi} = L(i\omega) \sum_{n=1}^N \frac{\Sigma_n S_n(q) + i\Delta_n T_n(q)}{B^n} + B. \quad (31)$$

We can remove ϕ by multiplying each term by its conjugate. Finally, multiplying by B^{2N} the equation can be easily rewritten as a $(N+2)$ -degree polynomial in the variable B whose coefficients depend only on the variable q

$$p(B) = \sum_{n=1}^{2N+2} C_n(q) B^n = 0. \quad (32)$$

It can be shown that $C_{2N+2} = 1/|L(i\omega)|^2$, $C_{2N+1} = 0$ and $C_{2N} = -\Gamma^2$. For sufficiently large q (that is when the interaction is negligible) we have that $C_k \cong 0$, $\forall k < 2N$, therefore

$$p(B) \cong (|L(i\omega)|^{-2} B^2 - \Gamma^2) B^{2N} = 0. \quad (33)$$

One root of the equation above is $B \cong \Gamma |L(i\omega)|$. This solution corresponds to the free oscillation amplitude that the cantilever assumes when the sample is far away and does not influence the cantilever dynamics. For every $q > 1$, the polynomial equation (32) can be solved in B . Only the solutions that are real and positive have relevance. The constant component of the periodic solution A can be evaluated exploiting the first of (30). The phase ϕ can also be similarly obtained as a function of the parameter q

$$\phi(q) = \arg \left\{ L^{-1}(i\omega) + \sum_{n=1}^N \frac{\Sigma_n S_n(q) + i\Delta_n T_n(q)}{B^{n+1}} \right\}. \quad (34)$$

Finally, the parameter l is given by the original relation

$$l(q) = qB(q) - A(q). \quad (35)$$

The final result is that the variables A , B , ϕ and l are all expressed with respect to the parameter q . The separation-amplitude diagram can be obtained considering the pair $(l(q), B(q))$ which describes a curve in a parametric form. A similar procedure can be used to obtain the relation between any two variables with no need of simulation tools.

In [17] and [16] it is shown that the approximation error of the HB method for the analysis of this model is negligible when compared to results obtained by simulating the same model.

5 Identification of the Tip-Sample Force Model

In this section we present methods to identify parameters of the hysteresis based models developed in earlier. As previously discussed, the frequency response $L(i\omega)$ is known since it can be independently estimated. We also assume that the separation l can be changed by means of the piezoactuator placed beneath the sample. Therefore, we can consider a set of M experiments with different values of l

$$l_m := l_0 + md \quad m = 1, \dots, M \quad (36)$$

where l_0 is a fixed offset and $d > 0$ is a suitable separation step. For every l_m the quantities A_m, B_m, ϕ_m can be evaluated from the measured signal $y(t)$ after it has reached its steady state, and q_m can be computed from (17).

The functions (8) chosen to model the interaction have the useful property that it is linear in the parameters K_n^- and K_n^+ , or in virtue of 16 and 19, Σ_n and Δ_n . The linear dependence on the parameters aids their identification using the harmonic balance relations (22). The first order harmonic balance equations lead to a set of M linear equations in the $2N$ unknown variables Σ_n and Δ_n

$$\begin{cases} \Gamma \cos(\phi_m) - \text{Im}[L^{-1}(i\omega)]B_m = \sum_{n=1}^N \Sigma_n \frac{S_n(q_m)}{B^{n+1}} \\ \Gamma \sin(\phi_m) - \text{Re}[L^{-1}(i\omega)]B_m = \sum_{n=1}^N \Delta_n \frac{T_n(q_m)}{B^{n+1}} \end{cases} \quad m = 1, \dots, M \quad (37)$$

Assuming that there are $M > 2N$ experimental measures and adopting a more compact notation, we can write two independent matrix equations

$$\begin{aligned} P_S \Sigma &= Q_S \\ P_D \Delta &= Q_D \end{aligned} \quad (38)$$

where

$$\Sigma := \begin{pmatrix} \Sigma_1 \\ \vdots \\ \Sigma_N \end{pmatrix} \quad \Delta := \begin{pmatrix} \Delta_1 \\ \vdots \\ \Delta_N \end{pmatrix} \quad (39)$$

are the unknown vectors and

$$\begin{aligned} P_S[m, n] &:= \frac{S_n(q_m)}{B_m^{n+1}} & Q_S[m] &:= \Gamma \cos(\phi_m) - \text{Re}[L^{-1}(i\omega)]B_m \\ P_D[m, n] &:= \frac{T_n(q_m)}{B_m^{n+1}} & Q_D[m] &:= \Gamma \sin(\phi_m) - \text{Im}[L^{-1}(i\omega)]B_m \end{aligned} \quad (40)$$

are constant matrices.

Since the number of equations is greater than the number of unknowns, (38) is

not expected to be feasible. A common strategy is to find the set of parameters which better “fits” the equations according to the quadratic cost function

$$V(l_0, \Sigma, \Delta) = \|Q_S - P_S \Sigma\|^2 + \|Q_D - P_D \Delta\|^2, \quad (41)$$

where we have stressed the dependence on the offset l_0 since it is not apriori known. Thus, the optimal values $\tilde{\Sigma}$ and $\tilde{\Delta}$ can be evaluated casting an optimization problem which also takes into account the constraints (9)

$$\begin{aligned} (\tilde{\Sigma}(l_0), \tilde{\Delta}(l_0)) &= \arg \min_{\Sigma, \Delta} V(l_0, \Sigma, \Delta) \\ &\text{subject to} \\ \Delta &\leq 0. \end{aligned} \quad (42)$$

We remark that forcing the condition $\Delta = 0$ in (42) is equivalent to the assumption of a interaction force with no hysteresis and therefore conservative.

Given l_0 , problem (42) is a quadratic optimization problem with linear constraints. Many algorithms are known in literature to determine its solution $(\tilde{\Sigma}(l_0), \tilde{\Delta}(l_0))$ [18]. Finally, we can estimate the offset l_0 by solution of the following problem

$$\tilde{l}_0 = \arg \min_{l_0} V(l_0, \tilde{\Sigma}(l_0), \tilde{\Delta}(l_0),) \quad (43)$$

which is another minimization over a scalar variable, solvable using a grid strategy. The identified parameters are $(\tilde{\Sigma}(\tilde{l}_0), \tilde{\Delta}(\tilde{l}_0))$.

6 Experimental Results

An atomic force microscope was operated in dynamic mode using a silicon cantilever of 225 μm in length. Using a thermal-response based approach the can-

tilever has been identified with a second order linear oscillator with natural frequency $\omega_n = 2\pi 73.881 \text{ rad/s}$ and damping factor $\xi = 0.00378$. The spring constant K of the cantilever has been estimated to be $4nN/nm$. A sinusoidal voltage with frequency ω_n has been applied to the dither piezo in order to make the cantilever oscillate. Experiments were performed on a silicon wafer sample. The separation amplitude curve has been experimentally measured during the two phases: approach and retract. Both curves show a jump phenomenon occurring at two close but different values of the separation (dashed and dotted curves in Figure 5). Such phenomena are present and documented in literature [6]. The identification technique described in the previous section has been employed using the data obtained during the retract phase only, while the data acquired during the approaching phase have been used for validation purposes. The results obtained using the piecewise linear interaction model are reported in Figure 5 (solid curve). The retract curve is well explained by the model data; this is not surprising as the data used to obtain the model parameters is the retract phase data. For the approach curve, a jump phenomenon occurring at a different separation is qualitatively well-predicted, but it can be argued that it is not quantitatively satisfactory.

As a second case, the following simplified model than (8) is used

$$h(\delta, \dot{\delta}) = \begin{cases} \frac{K_7^-}{\delta^7} + \frac{K_{13}^-}{\delta^{13}} & \text{if } \dot{\delta} < 0 \\ \frac{K_7^+}{\delta^7} + \frac{K_{13}^+}{\delta^{13}} & \text{if } \dot{\delta} > 0 \end{cases} \quad (44)$$

that is a standard 6 – 12 Lennard-Jones potential function with a hysteresis dissipation. Identification results are shown in Figure 6. As it is evident from

the figure, the model predicts the discontinuity in the approach phase of the force curve accurately. The phase of the first harmonic is also predicted well by the model.

As remarked in Figures 5 and 6, harmonic balance has also allowed to reveal the presence of instable periodic orbits (in the region in between the two jump points) and to clearly explain bifurcation phenomena in the system.

7 Conclusions

In the paper we have proposed a class of models for tip-sample interaction in atomic force microscopy via impact dynamics. The use of a hysteresis can be well combined with harmonic balance techniques for the analysis of oscillatory behaviour to provide interesting insights into the dynamics. For instance, the presence of jump phenomena discovered in many experiments is well-predicted and explained. The suggested method is based on a first order harmonic approximation and gives good quantitative results since the linear part of the considered Lur'e system shows a sharp filtering effect near the resonance frequency. In such a situation, the Harmonic Balance technique has advantages over standard numerical approaches since it requires a computational effort much smaller than the one required by simulation tools.

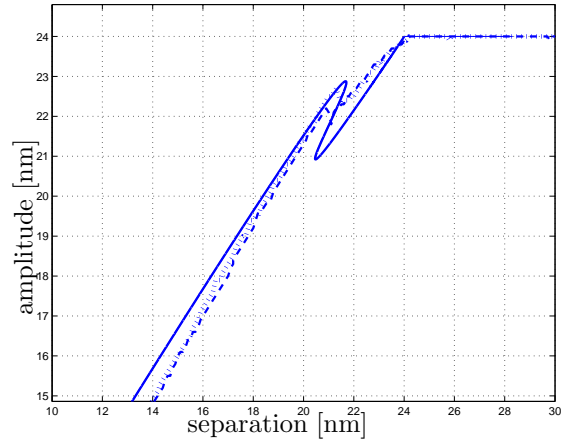
References

- [1] B. Brogliato. *Nonsmooth Mechanics: Models Dynamics and Control*. Springer Verlag, New York, 1999.
- [2] R. Brach. *Mechanical Impact Dynamics: Rigid Body Collisions*. Wiley, New York, 1991.
- [3] P. Fontaine, P. Guenon, and J. Daillant. A critical look at surface force measurement using a commercial atomic force microscope in the noncontact mode. *Rev. Sci. Instrument.*, 68:4145–4151, 1997.
- [4] H. K. Khalil. *Nonlinear Systems*. Prentice-Hall, Upper Saddle River, 1996.
- [5] J. N. Israelachvili. *Intermolecular and Surface Forces*. Academic Press, New York, 1985.
- [6] A. Kyhle, A. H. Sorensen, and J. Bohr. Role of attractive forces in tapping tip force microscopy. *Journal of Applied Physics*, 81:6562–6569, 1997.
- [7] A. Sebastian, M. Salapaka, and D. Chen. Harmonic and power balance tools for tapping-mode afm. *Journal of Applied Physics*, 89:6473–6480, 2001.
- [8] H. Holscher. Quantitative measurement of tip-sample interactions in amplitude modulation atomic force microscopy. *Applied Physics Letters*, 89:123109, 2006.

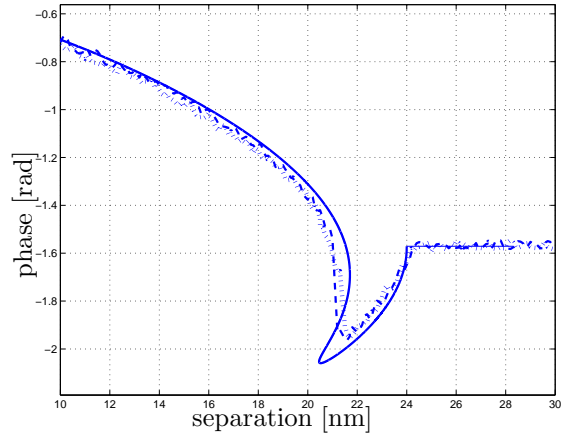
- [9] M. Salapaka, D. Chen, and J. Cleveland. Linearity of amplitude and phase in tapping-mode atomic force microscopy. *Physical Review B*, 61:1106–1115, 2000.
- [10] B. Cappella and G. Dietler. Force distance by atomic force microscopy. *Surface Science Reports*, 34:1–104, 1999.
- [11] M. Basso, R. Genesio, A. Tesi, and G. Torrini. On describing systems with periodic behaviour in terms of simple nonlinear models. In *Proc. of Conference Control of Oscillations and Chaos*, Saint-Petersburg (Russia), August 1997.
- [12] M. Basso, R. Genesio, and A. Tesi. A frequency method for predicting limit cycle bifurcations. *Nonlinear Dynamics*, 13:339–360, 1997.
- [13] C. Gibson, D. Smith, and C. Roberts. Calibration of silicon atomic force microscope cantilevers. *Nanotechnology*, 16:234–238, 2005.
- [14] M. Lee and W. Jhe. General theory of amplitude-modulation atomic force microscopy. *Physical Review Letters*, 97:036104, 2006.
- [15] R. Garcia, C. J. Gomez, N. F. Martinez, S. Patil, C. Dietz, and R. Magerle. Identification of nanoscale dissipation processes by dynamic atomic force microscopy. *Physical Review Letters*, 97:016103/1–4, 2006.
- [16] D. Materassi, M. Basso, and R. Genesio. Frequency analysis of atomic force microscopes with repulsive-attractive interaction potentials. In *Proc.*

of IEEE Conference on Decision and Control, Paradise Island (Bahamas),
December 2004.

- [17] M. Basso and D. Materassi. Frequency analysis and identification in atomic force microscopy. Technical report, Dipartimento di Sistemi e Informatica, 2006.
- [18] S. Boyd and L. Vandenberghe. *Convex Optimization*. Cambridge University Press, Cambridge, 2004.

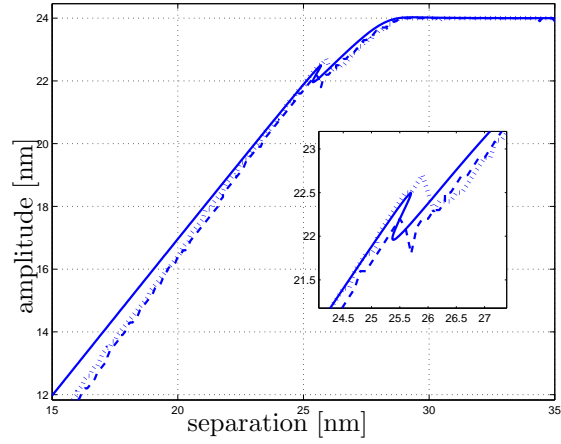


(a)

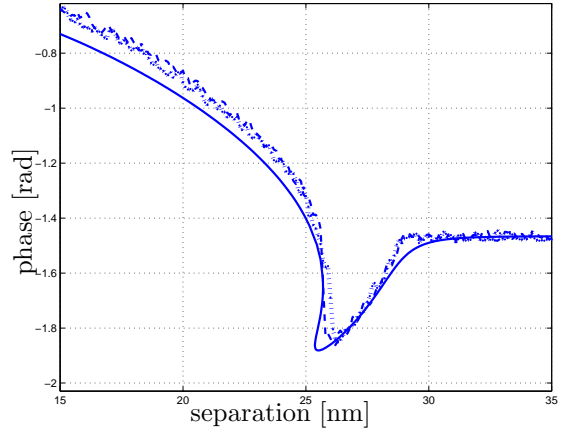


(b)

Figure 5: Experimental separation-amplitude (a) and separation-phase (b) curves fitted using the piecewise linear model for the interaction force. Solid line is the curve obtained by the model; the dashed and the dotted ones are the experimental approach and retract curves respectively.



(a)



(b)

Figure 6: Experimental separation-amplitude (a) and separation-phase (b) curves fitted using the Lennard-Jones model for the interaction force. Solid line is the curve obtained by the model; the dashed and the dotted ones are the experimental approach and retract curves respectively.

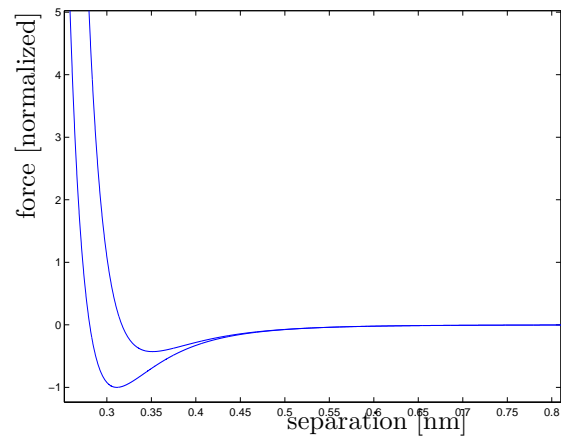


Figure 7: Identified dynamic Lennard-Jones force curve with hysteresis.